Journal of Solid State Electrochemistry (2019) 23:1593–1604
https://doi.org/10.1007/s10008-019-04240-6

ORIGINAL PAPER

Effect of silver coating on electrochemical performance of $0.5Li_2MnO_3.0.5\ LiMn_{1/3}Ni_{1/3}Co_{1/3}O_2$ cathode material for lithium-ion batteries

Halil Şahan[1,2] · Hüseyin Göktepe[2] · Şaban Patat[2] · Süleyman Yıldız[2] · Burcu Özdemir[2] · Ahmet Ülgen[2] · Sanjeev Mukerjee[1] · K. M. Abraham[1]

Received: 25 November 2018 / Revised: 10 March 2019 / Accepted: 11 March 2019 / Published online: 3 April 2019

Abstract

In this work, a Li-rich layered $0.5Li_2MnO_3.0.5LiMn_{1/3}Ni_{1/3}Co_{1/3}O_2$ (LMNCO) pristine cathode material synthesized with a glycine-nitrate combustion method is further coated with silver. The effects of silver coating on the material structure and performance of the as-prepared cathode are systemically studied with X-ray diffraction (XRD), scanning electron microscope (SEM), galvanostatic charge/discharge, cyclic voltammetry (CV), and electrochemical impedance spectra (EIS). Material characterizations and electrochemical measurements show that the surface modification does not lead to the change of crystal lattice parameter and particle morphology. It is found that the rate capability and cyclability can be significantly improved, which could be attributed to the enhancement of electronic conductivity of the particle surface of the cathode. It has been found that the obtained silver-coated LMNCO cathode exhibits excellent electrochemical characteristics. For example, it can deliver a high initial discharge capacity of 290 mAh g^{-1} between 2.0 and 4.9 V at a rate of 0.05C at room temperature and a discharge capacity of 159 mAh g^{-1} at 1 C, 128 mAh g^{-1}at 2 C, and 101 mAh g^{-1} even at 5 C. EIS result shows that R_{sf} and R_{ct} values of LMNCO are bigger than those of silver-coated LMNCO cathode.

Keywords Li-rich layered cathodes · Lithium batteries · Silver coating · Capacity fade · Cycling performance · Cyclic voltammetry

Introduction

Nowadays, rechargeable Li-ion batteries (LIBs) are extensively used in almost all types of electronic devices, including cell phones, laptop computers, camcorders, and even electric and hybrid electric vehicles due to their high energy and power density, high voltage, and long lifespan [1–3]. The LIBs materials for new generations of such apparatuses are required for combining high power and energy densities. In the three primary functional components of the lithium-ion battery, cathode material plays a decisive role on its electrochemical properties. Since 1991, the cathode material $LiCoO_2$ was commercialized by Sony Corporation, but $LiCoO_2$ has limitations with respect to capacity, thermal stability, high cost, and chemical stability at high states of charge (above 4.3 V). Therefore, there is a strong demand to find some new alternative cathode materials to solve these problems [2, 4, 5]. Layered lithium transition metal oxide $LiNi_{1-x-y}Co_xMn_yO_2$ has been regarded as the most important cathode material for high-energy batteries due to their intrinsic characteristics, such as less toxicity, lower cost, better thermal stability, and higher discharge capacity than currently large-scale used $LiCoO_2$ [6–8].

In particular, "layered–layered" $xLi_2MnO_3\cdot(1-x)LiMn_{1/3}Ni_{1/3}Co_{1/3}O_2$ lithium-rich manganese–based solid solution cathode materials, which are comprised of a two-layered component, are known to deliver a discharge capacity of 200–250 mAh g^{-1} when charged to high potentials, and their capacities are almost twice than that of a conventional Li_xCoO_2 electrode [9, 10].

✉ Halil Şahan
halilsahan77@gmail.com

[1] Center for Renewable Energy Technology, Department of Chemistry and Chemical Biology, Northeastern University, Boston, MA 02115, USA

[2] Science Faculty, Deparment of Chemistry, Erciyes University, 38039 Kayseri, Turkey

However, "layered–layered" $xLi_2MnO_3 \cdot (1-x)LiMn_{1/3}Ni_{1/3}Co_{1/3}O_2$ lithium-rich manganese–based solid solution cathode materials still have several performance drawbacks, such as

1. Large irreversible capacity loss (20–30%) in the first cycle,
2. Poor rate capacity performance,
3. Poor cycling stability, especially at high current density [11].

The mechanical degradation is mainly due to the fracture of electrode materials especially for those with high energy density, finally leading to the loss of electrical contact [12]. On the other side, the chemical degradation is mainly associated with the aggravated side reactions between the cathode materials and the electrolyte under high voltage which results in the formation of a non-conducting solid electrolyte interface layer, accelerating damage to the cathode material surface [13, 14]. Abraham et al. report on solutions to three of the aforementioned deficiencies of the lithium-rich layered–layered composite oxides by substituting some of the Li with Na [15]. One effective method to resolve the aforementioned problems of lithium-rich materials is surface modification with coating materials such as Al_2O_3, ZrO_2, MoO_3, and AlF_3, which reduces the irreversible capacity in the initial cycle and improves cyclic stability by suppressing elimination of oxygen-ion vacancies and parasitic reactions at high voltage (≥ 4.5 V) [16–19]. Recently, the silver coating was reported to improve the rate performance and cyclic stability of $LiMn_2O_4$ and $LiFePO_4$ [20, 21].

In this study, we first prepared $Li_{1.3}Mn_{0.666}Ni_{0.167}Co_{0.167}O_{2.4}$ ($0.5Li_2MnO_3.0.5\ LiMn_{1/3}Ni_{1/3}Co_{1/3}O_2$) (LMNCO) with silver nanocoating which remarkably enhanced the electrochemical performances of LMNCO including cyclic stability and rate capability. The improved electrochemical performance together with the low-cost nature and simple preparation approach makes it possible to use these new $0.5Li_2MnO_3.0.5\ LiMn_{1/3}Ni_{1/3}Co_{1/3}O_2$ composite materials as promising cathode candidate in lithium-ion batteries.

Experimental

Synthesis of $0.5Li_2MnO_3.0.5\ LiMn_{1/3}Ni_{1/3}Co_{1/3}O_2$ cathode

Untreated LMNCO was synthesized with a glycine–nitrate combustion process. Figure 1 shows the preparation procedure of the cathode material. Firstly, stoichiometric amounts

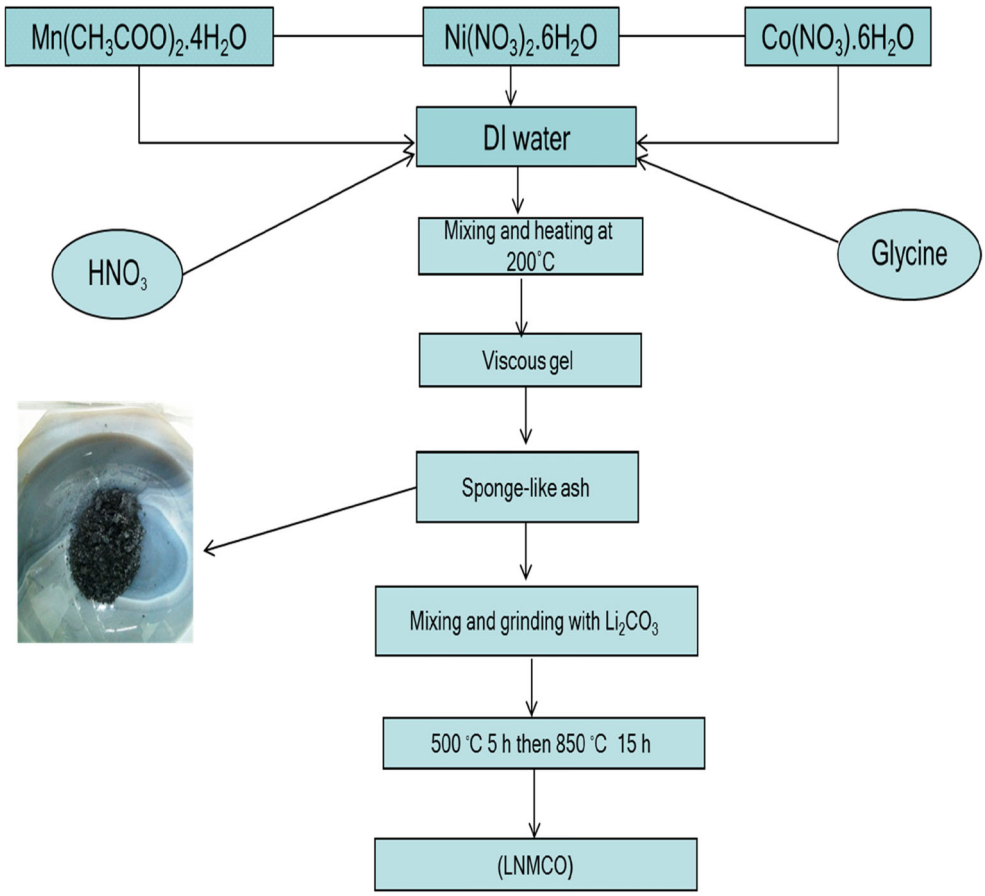

Fig. 1 Synthesis procedure of LMNCO cathode

of $Mn(CH_3COO)_2{\cdot}4H_2O$ (Sigma), $Co(NO_3)_2.6H_2O$ (Merck), and $Ni(NO_3)_2.6H_2O$ were dissolved in distilled water. Glycine (Merck) was added to the solution either as a solid or as a water solution. Its role was to serve both as a fuel for combustion and as a complexant to prevent inhomogeneous precipitation of individual components prior to combustion. Finally, nitric acid with the same mole of acetate anions was added to the solution. The solution was heated continuously without any previous thermal dehydration. Afterwards, the solution became a transparent viscous gel which was auto-ignited, giving a voluminous, black, and sponge-like ash product of combustion. The resulting ash was mixed and grinded with a stoichiometric amount of Li_2CO_3 and then, it was heated at 500 °C for 5 h, 850 °C for 15 h in air, respectively. In order to coat LNMCO with silver, silver nitrate was solved in the mixture of ethanol and deionized water, and then, LNMCO powder was added into the solution. The cathode was suspended in the solution which was stirred vigorously with a magnetic stirrer. Finally, ammonia solution (25 *w*/*w* %) was poured in this suspension to reduce silver ions and thereby deposit metallic silver particles on the LNMCO powder. The weight ratio of the silver nitrate to the LNMCO powders for this method was 5 wt%. The above composition and synthesis of silver-coated $LiMn_2O_4$ samples were fixed by Son in earlier studies [20].

Characterization techniques

The crystal pattern of the samples was characterized with X-ray diffractometer (Rigaku Ultima IV) equipped with Cu-Kα radiation ($\alpha = 1.54178$ Å) and a graphite monochromator. Scanning electron microscope (SEM, Zeiss EVO) and field-emission scanning electron microscope (FESEM, Hitachi S-4800) were used to observe the morphology of the powders by equipping energy dispersive spectroscopy (EDS) to performed element composition of the powders. The silver component in the coated sample was determined with an inductively coupled plasma (ICP) emission spectrometer (Agilent 7500A). Thermal analysis of the precursor sample (ash and Li_2CO_3) of cathode material was carried out using a Pekin Elmer (diamond) TG/DTA thermal analyzer at a heating rate of 10 °C min^{-1} under air atmosphere to specify the optimum temperature for phase formation of LMNCO.

Electrochemical measurements

The electrode slurry was produced by mixing active materials with polyvinylidene fluoride (PVDF was dissolved in *N*-methyl-2-pyrrolidone (NMP) with a content of 10 wt%) as a binder and Super P carbon black as a conductive agent with a weight ratio of 8:1:1. This slurry was coated onto Al foils via doctor blade technique and then dried at 120 °C for overnight in a vacuum oven. Each electrode was cut into discs with a diameter of 11 mm. The final working electrodes were usually discs whose active mass exposed to the electrolyte solution were 4–5 mg cm^{-2}. Electrochemical measurements were performed using Swagelok-type cells with lithium foil as the counter/reference electrode, and glass microfiber filters (Whatman) as the separator. The electrolyte was a 1 M $LiPF_6$ solution in a 50:50 (*w*:*w*) mixture of ethylene carbonate (EC) and diethyl carbonate (DEC). The cells were assembled in argon-filled MBraun Uni Lab glovebox. All the as-prepared cells were stabilized for 5 h before measurements. The cells were galvanostatically charged and discharged on an 8 channel MTI battery analyzer. The cells were typically cycled between 2.0 to 4.9 V vs Li^+/Li^0, and 1.0 C rate was equal to the current density of 280 mA g^{-1}. Cyclic voltammograms (CV) and electrochemical impedance spectroscopy (EIS) measurements were performed with a VersaSTAT MC multi-channel potentiostat/galvanostat/impedance analyzer. CV tests were investigated in the voltage range of 2.0–5.0 V at a scan rate of 0.1 mV s^{-1}, and EIS tests were carried out when the amplitude of AC signal was 5 mV over a frequency range from 100 kHz to 10 mHz at 4.1 V charge state. Electronic conductivity of cathodes was measured with a linear scanning voltammetry method with a VersaSTAT MC multi-channel potentiostat/galvanostat/impedance analyzer.

Results and discussion

The TG/DTA curve of LMNCO precursor is described in Fig. 2. In order to better find out the decomposition reactions occurring in the synthesis, TG analysis was fulfilled on the precursor sample at a ramp rate of 10 °C min^{-1}. The TG curve clearly displays the three weight loss regions. The mass loss between 100 and 200 °C is attributed to the physically adsorbed water from the precursor mixture. Further, the TG curve shows steep weight loss between 450 and 600 °C. This effect is due to the thermal decomposition of Li_2CO_3.

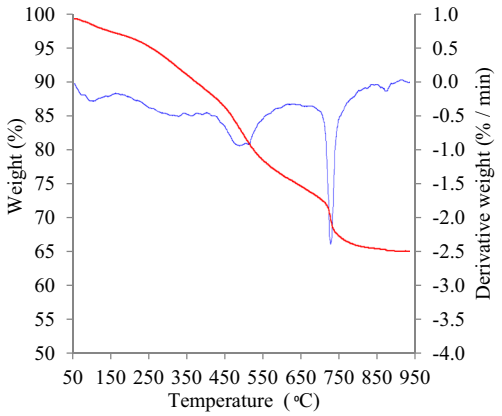

Fig. 2 Thermogravimetric and differential thermal analysis (TG/DTA) of the precursor sample (ash and Li_2CO_3)

Although pure Li_2CO_3 decomposes around 750 °C, as earlier studies [22] have indicated, this result suggests that the decomposition temperature can be imposed by the presence of water and transitional metals. Finally, TG/DTA curve presents a well-defined exothermic peak at 730 °C suggesting the formation of layered material. DTA curve advocates no further thermal reactions beyond 800 °C.

The XRD patterns of the pristine and silver-coated LMNCO prepared with combustion method are presented in Fig. 3. All the diffraction peaks can be indexed as the a-$NaFeO_2$-type layered structure (space group R-3m) with additional weak short-ranged super structure reflections around $2\theta = 20–25°$. The characteristic diffraction peaks of silver cannot be seen in the XRD pattern due to the low weight ratio of silver (0.93 wt%) in the cathode material. The weak peaks between 20 and 25° are consistent with the $LiMn_6$ cation arrangement that occurs in the transition metal layer of Li_2MnO_3. The (006)/(102) and (108)/(110) doublets are clear

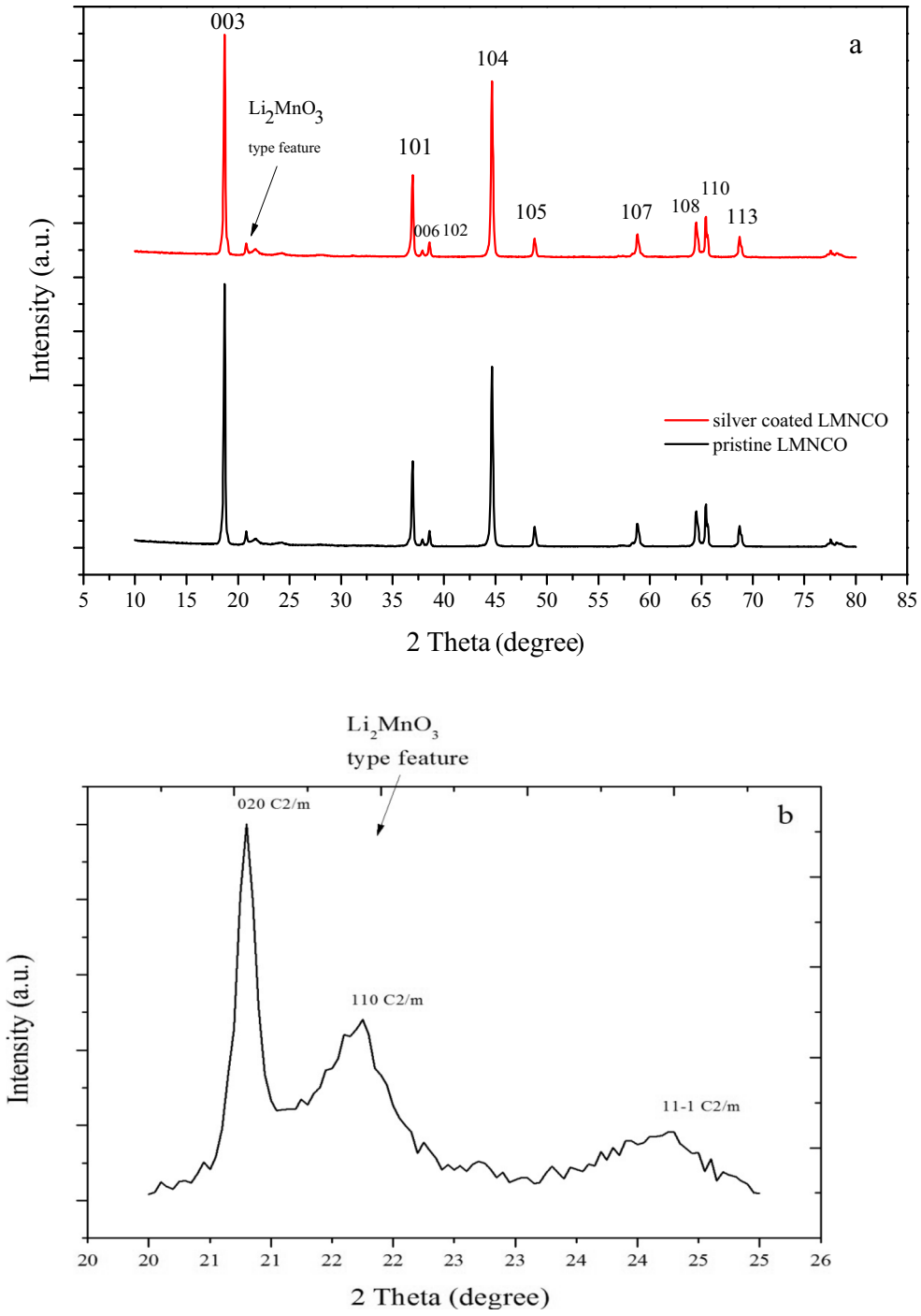

Fig. 3 XRD patterns (**a**) of the obtained samples and its partial magnification (**b**)

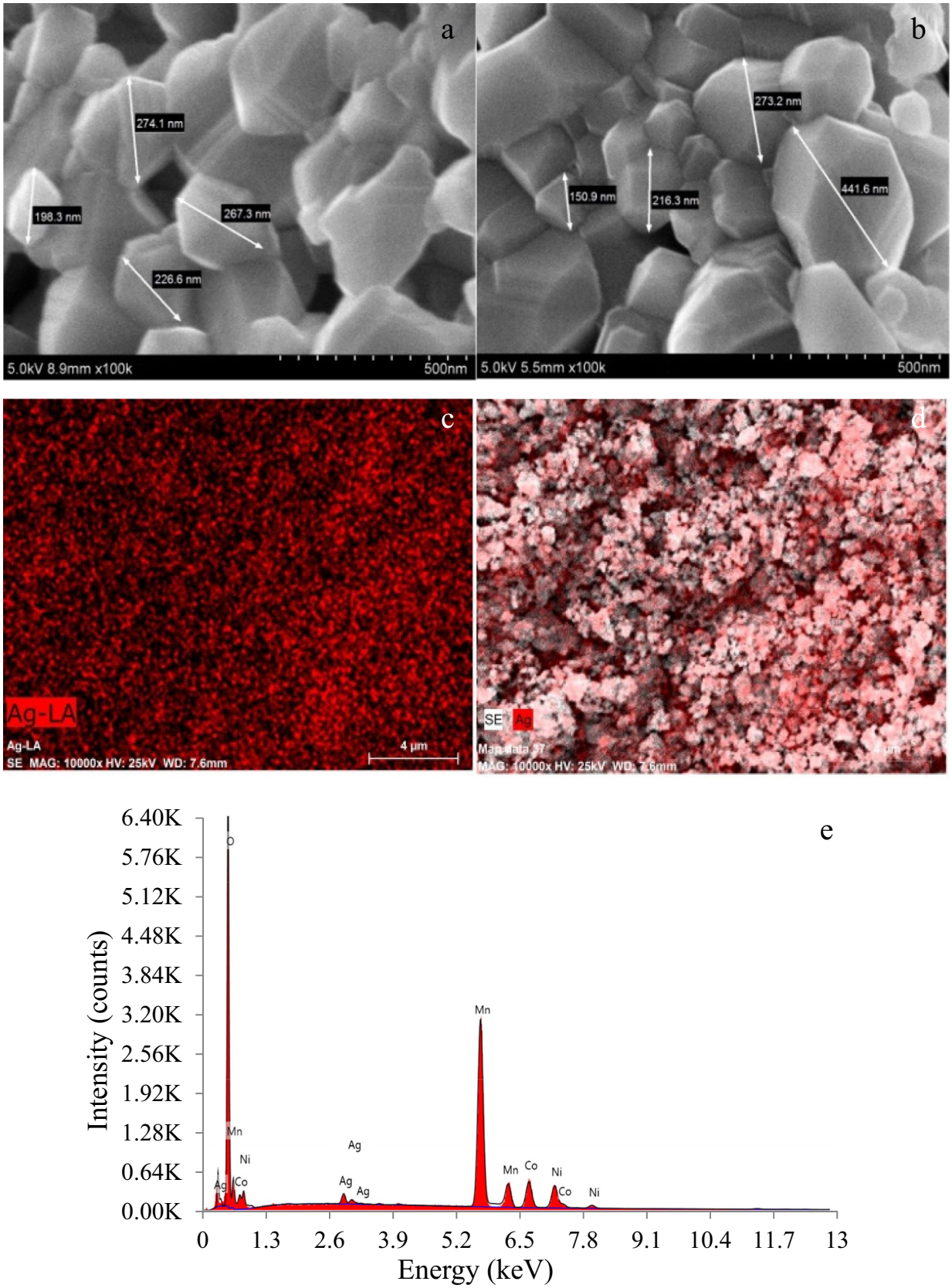

Fig. 4 **a**, **b** SEM micrograph of pristine LNMCO and silver-coated LMNCO powders. **c**, **d** Mapping of silver-coated LMNCO and **e** EDS spectrum result of silver-coated LMNCO

split, which indicates the as-prepared layered structures have good hexagonal ordering [23]. The ratio of $I(003)/I(104)$ is 1.423 (> 1.2), which also demonstrates the formation of layered structure, and the cation mixing phenomenon is very weak [24]. Lattice constants were calculated from the XRD pattern of Fig. 3 with a least-squares refinement. The lattice constants of pristine and silver-coated LMNCO were determined to be 0.2850(3) nm and 0.2820(4) nm for (a), and 1.4238(2) nm and 1.4242(2) nm for (c) with a unit volume of 0.11156 nm^3 and 0.11325 nm^3, using only the R3m space group during Rietveld refinements, respectively. The crystal size parameter of LMNCO from the XRD data via the Williamson–Hall method was found as a 45.69(4) nm.

The SEM images of the LMNCO and silver-coated LMNCO materials are shown in Fig. 4. Figure 4a and b reveal that the polyhedral-spherical nanoparticle of pristine and silver-coated LMNCO powder is relatively uniform in the range from 100 to 500 nm. The sharp edges and smooth planes indicate that the LMNCO material is highly crystallized, which is consistent with the XRD results. The formation of the polyhedral-spherical particle is beneficial for achieving a high tap density and energy density. In addition, it should be noted that, in cathode materials, the Li^+-ion diffusion not only adheres to the size of primary particles but also to on the morphology and porosity of the secondary particles.

Figure 4 e shows EDS analysis and elemental mapping of silver-coated LMNCO cathode. As seen in Fig. 4 c–d, silver is homogeneously distributed onto LMNCO cathode material. Furthermore, to verify the chemical composition of the synthesized particles, the EDS analysis of silver-coated LMNCO sample with SEM was conducted. EDS spectrum of the sample exhibits the characteristic peaks of Mn, Ni, Co, O, and Ag. No other element was detected in EDS analysis with SEM. From the EDS spectrum, the weight ratio of silver in the cathode material was calculated to be below 2.0%. Because of the fact that EDX is a semiquantitative analysis method, we carried out ICP analysis in order to determine the real silver content in the cathode material. ICP analysis revealed that the weight ratio of silver was 0.93%. The stoichiometric factor of $Ag/AgNO_3$ is 0.63. Reduced metallic silver particles may not deposit on the surface of cathode particles and may migrate into the coating solution during the coating process. Because of these reasons, the silver content in the cathode material has a low ratio.

Figure 5 a, b represents the initial charge–discharge profile of LMNCO and silver-coated LMNCO cathodes at a current density of 0.05 C (1.0 C = 280 mA g^{-1}) in the voltage range of 2.0–4.9 V at room temperature. As can be seen in Fig. 5, there are two plateaus in the initial charge profile: one is at about 4.0 V and the other one is at about 4.5 V. The former plateau is the Li-extraction from the structure of space group *R-3m* accompanying the reactions of $Ni^{2+/4+}$ and $Co^{3+/4+}$ [25].

As expected, the potential plateau during the first charge is much shorter and the capacity delivered is less for the pristine electrode (278 mAh g^{-1}), whereas the first discharge capacity for silver-coated LMNCO cathode was found as 290 mAh g^{-1} at 0.05 C rate. Besides, the 5th, 35th, and 65th discharge capacities of pristine cathode were found as 140.1 mAh g^{-1}, 85.6 mAh g^{-1}, and 42.8 mAh g^{-1} at 1 C, 2 C, and 5 C, respectively. On the other hand, the 5th, 35th, and 65th discharge capacities of silver-coated cathode were found as 158.1 mAh g^{-1}, 127.5 mAh g^{-1}, and 97.3 mAh g^{-1} under the same condition. It can be clearly said that the improvement of the discharge capacities at different C rates is related to increasing the conductivity of cathode. It is believed that silver surface modification not only reduced the side reactions but also significantly enhanced the surface intercalation reaction and reduced the polarization in the cell.

Figure 5 c shows several charge–discharge profiles (5th–20th) of the pristine and silver-coated cathode at 1 C rate. It can be clearly seen in Fig. 5 c that the gaps occupy the space between the charge and discharge plateau regions. The gaps which are related to polarization in the cell are different in sizes. The gap for the pristine cathode is much bigger than that for the silver-coated cathode. This means that the polarization of pristine cathode increases with cycling, whereas the polarization of silver-coated cathode is nearly the same. These results revealed that silver coating decreased both polarization and voltage level of the cell.

All cathodes were charged at 0.05 C rate and discharged at 1 C rate for the first 50 cycles, then charged/discharged at 1 C rate for the second 50 cycles. Results are compared in Fig. 5 d. The silver-coated pristine cathode maintains 146.4 mAh g^{-1}, which corresponds to 84% of the initial capacity after the first 50 cycles. The discharge capacity of the pristine cathode seriously fades, and only 65% is retained after the first 50th cycle. In addition, after the second 50 cycles (100th cycle), the discharge capacity and capacity retention of pristine and silver-coated cathodes are 90.4 mAh g^{-1}, 124.6 mAh g^{-1}, and 53%, 71%, respectively. As can be seen Fig. 5 d, silver coating significantly improved cycling stability of cathode due to the enhancement of electron and ionic conductivity. This issue is related to the good electron transportation during the lithium insertion-extraction reaction of the cathode.

Rate performance tests were conducted between 2.0–4.9 V at 1 C (280 mA g^{-1}), 2 C (560 mA g^{-1}), and 5 C (1400 mA g^{-1}) for 30 cycles. The results of the rate

Fig. 5 **a**, **b** The charge–discharge profile of LMNCO and silver-coated LMNCO cathodes. **c** Specific capacity vs. voltage curves for the pristine and silver-coated electrodes at the 5th, 10th, 15th, and 20th cycle at 1 C rate. **d** Cycling behavior of LMNCO and silver-coated LMNCO cathodes at various charge rates and constant discharge rate measured in the potential range of 2.0–4.9 V. **e** Rate performance of LMNCO and silver-coated LMNCO cathodes in the potential range of 2.0–4.9 V

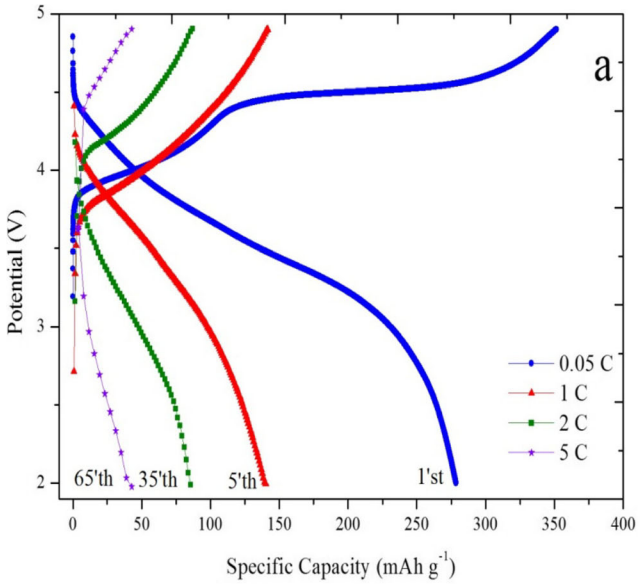
a
Potential (V)
Specific Capacity (mAh g-1)
0.05 C
1 C
2 C
5 C
65'th
35'th
5'th
1'st

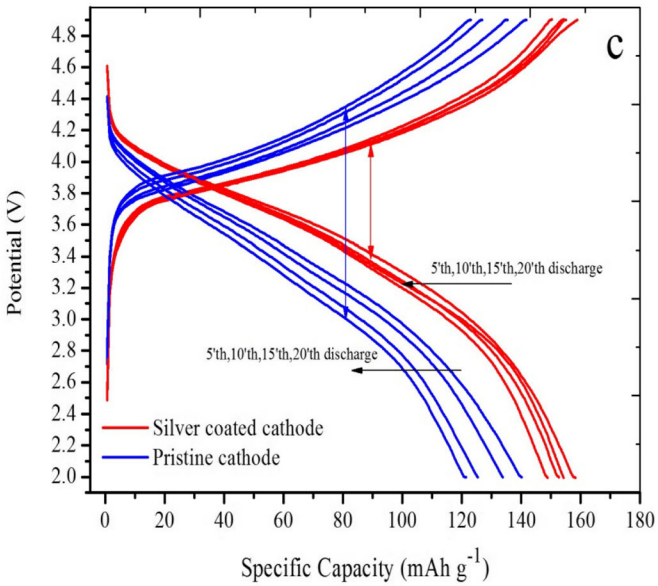
c
Potential (V)
Specific Capacity (mAh g-1)
5'th,10'th,15'th,20'th discharge
5'th,10'th,15'th,20'th discharge
Silver coated cathode
Pristine cathode

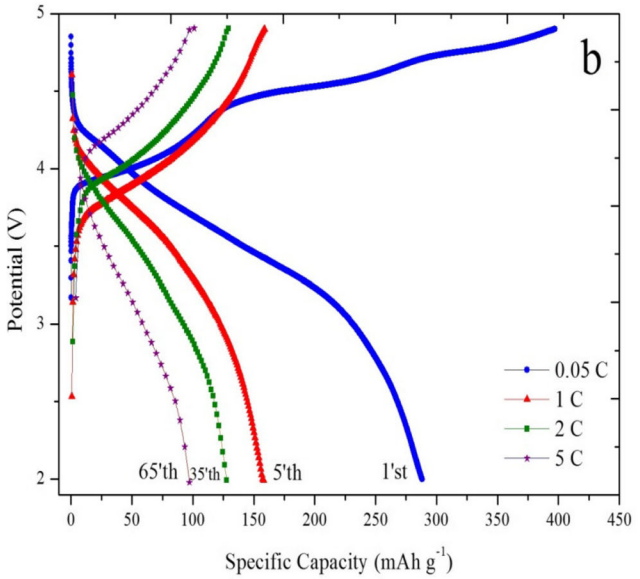
b
Potential (V)
Specific Capacity (mAh g-1)
0.05 C
1 C
2 C
5 C
65'th
35'th
5'th
1'st

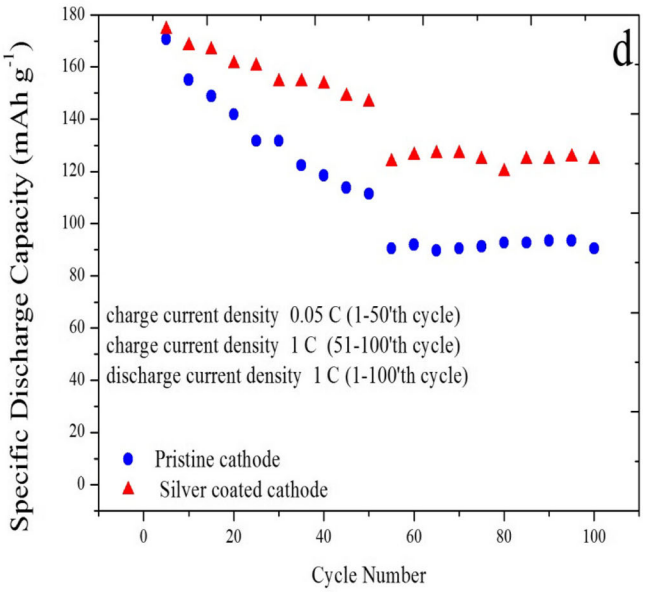
d
Specific Discharge Capacity (mAh g-1)
Cycle Number
charge current density 0.05 C (1-50'th cycle)
charge current density 1 C (51-100'th cycle)
discharge current density 1 C (1-100'th cycle)
Pristine cathode
Silver coated cathode

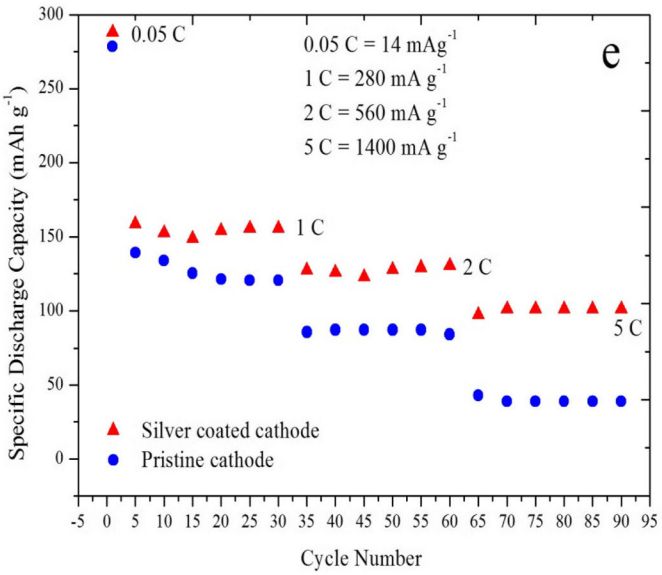
e
Specific Discharge Capacity (mAh g-1)
Cycle Number
0.05 C
0.05 C = 14 mAg-1
1 C = 280 mA g-1
2 C = 560 mA g-1
5 C = 1400 mA g-1
1 C
2 C
5 C
Silver coated cathode
Pristine cathode

capability tests of the LMNCO and silver-coated LMNCO cathode materials are compared in Fig. 5 e and Table 1.

The figure shows similar trends to those observed in the cycling tests. As seen in Fig. 5 e and Table 1, silver-coated cathode delivers a 30th, 60th, and 90th discharge capacity of 155.8, 130.6, and 101.1 mAh g^{-1} at 1 C, 2 C, and 5 C, respectively, which is obviously higher than the pristine cathode of 120.6, 84.1, and 38.9 mAh g^{-1} and what's more, the capacity fade ratios of silver cathode are lower than that of the pristine cathode. Rate performance tests revealed that the polarization of cathode can be hindered at high current densities via silver coating. The silver-coated cathode material shows better electrochemical performance and higher discharge capacities at all rates because it possesses better electronic conductivity. Electronic conductivity of pristine LMNCO and silver-coated LMNCO cathodes was found as 4.01×10^{-6} S cm^{-1} and 4.4×10^{-4} S cm^{-1}, respectively. The resistance (R) was extracted from the I–V curve based on Ohm's law. Resistivity (δ) was determined using the equation $R = \delta \frac{L}{A}$ where A is the pellet area and L is its thickness. 1/δ yielded dc electronic conductivity for each cathode.

The redox behavior of the LMNCO and silver-coated LMNCO cathodes were investigated with CV shown in Fig. 6. Before the cycling process, two primary peaks appeared at about 4.2 V and upon 4.5 V. The first peak can be attributed to the oxidation of Ni^{2+} and Co^{3+} to Ni^{4+} and Co^{4+}, respectively. The second peak beyond 4.5 V is due to Li_2MnO_3 activation where Li_2O is released from the structure, and the reduction peak appearing about 3.8 V could be related to Co^{4+} and Ni^{4+} reduction. After the activation of Li_2MnO_3, some new redox properties were seen in the first cycle. For instance, after the first cycling procedure, first new oxidation peaks appeared at around 3.3 V. This new peak which appeared at 3.3 V is probably due to the oxidation of reduced (lithiated) MnO_2 (from Mn^{3+} to Mn^{4+}) created in the first discharge. Subsequently, the second new oxidation peak appeared due mainly to Ni^{2+}/Ni^{4+} oxidation, and a small peak just below 4.5 V was determined which is attributed to the oxidation of Co^{3+}. These oxidation peaks are followed by reduction peaks which could be Co^{4+} and Ni^{4+} reduction at 3.7 V, respectively [26, 27]. Finally, the last reduction peak which is located around 3.3 V due to Mn reduction from partially oxidized Mn^{3+} appeared. In general, after the 30th cycle, the peaks shifted to lower potentials, a strong indication of structural transformation. Figure 6 extrapolated that redox behavior of the

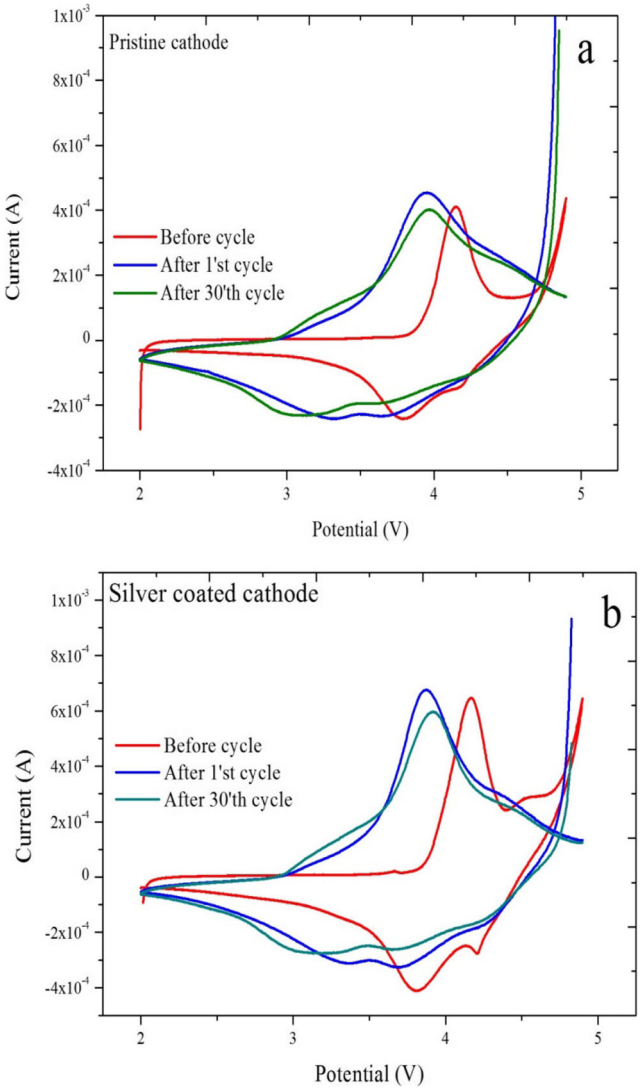

Fig. 6 Cyclic voltammograms of the LMNCO and silver-coated LMNCO cathodes recorded in the voltage range of 2.0–5.0 V at scan rate 0.1 mV s^{-1}

Table 1 Discharge capacity and capacity fade ratios of the pristine and silver coated cathodes at different C rates as shown in Fig. 5e

Cycle number / C-rate	Pristine cathode		Silver coated cathode	
	Discharge capacity (mAh g^{-1})	Capacity fade %	Discharge capacity (mAh g^{-1})	Capacity fade %
5'th / 1 C	139.3	13.4	158.9	2.0
30'th / 1 C	120.6		155.8	
35'th / 2 C	85.6	1.8	127.5	0.0
60'th / 2 C	84.1		130.6	
65'th / 5 C	42.8	9.1	97.2	0.0
90'th / 5 C	38.9		101.1	

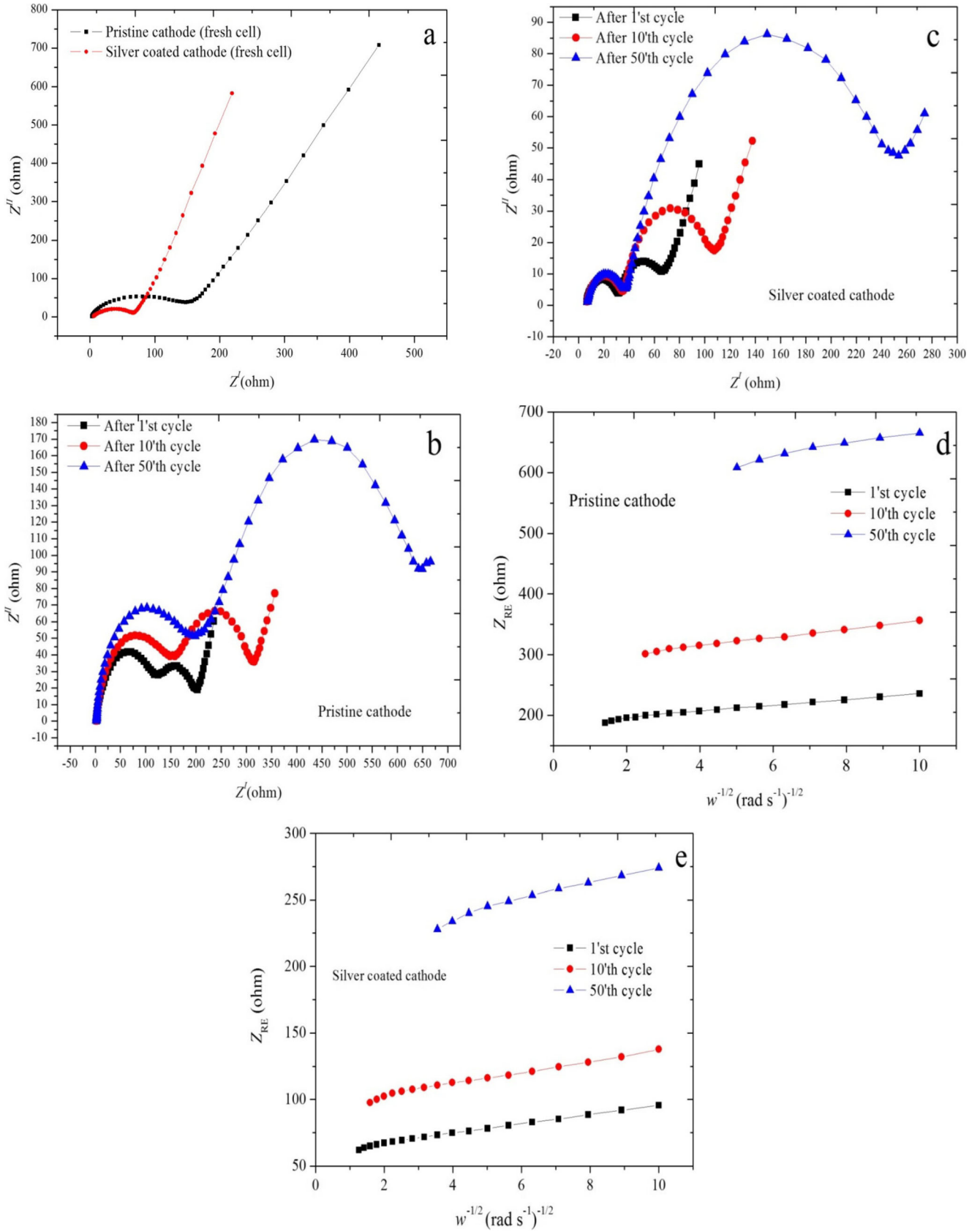

Fig. 7 **a**, **b**, **c** Electrochemical impedance spectroscopy (EIS) Nyquist plots of LMNCO and silver-coated LMNCO cathodes at 4.1 V. **d**, **e** Pristine cathode and silver-coated cathode for the relationship between Z_{RE} and $w^{-1/2}$ at low-frequency region

LMNCO and silver-coated LMNCO cathodes resemble each other. Because of this reason, it may be clearly stated that the silver coating process does not have a destructive effect on the electrochemical process. When we compare two different CV results, we can see that the redox peak intensity of silver-coated LMNCO cathode is sharper than the pristine one. This result may be related to better electrochemistry kinetics of coated cathode.

Electrochemical impedance spectroscopy (EIS) of the charged (4.1 V) Swagelock-type T cells is conducted to analyze the interface reaction and the process of lithium intercalation/de-intercalation into the electrode. The EIS profiles of the cathodes were obtained when the cell was fresh and for the cycles 1, 10, and 50 times respectively at 1 C between 2.0–4.9 V. The EIS spectrum of fresh cathodes shows that silver-coated LMNCO cathode has fewer impedance than a pristine one. It can be observed that each plot exhibits two arcs and one slope line. Commonly, the high-frequency semicircle reflects the impedance of lithium-ion diffusion in the surface layer (including SEI layer and surface modification layer) of the electrode (R_{sf}) [28]; the second semicircle in the intermediate frequency arc is related to charge transfer impedance in the electrode/electrolyte (surface film and the active cathode mass) interface (R_{ct}) [29]; and the sloped line of the low-frequency range is bound up with the Warburg impedance (Zw) which corresponds to lithium-ion diffusion in the material [30]. As seen in Fig. 7 b and c, the first semicircles which are related with SEI (R_{sf}) for the silver-coated cathode are almost similar. In stark contrast, the first semicircle of pristine cathode continuously increases with cycling. This means that lithium-ion diffusion of the pristine cathode in the surface layer continuously declines after the first cycle. It can be clearly said from the EIS measurements that silver-coated LMNCO cathode has more stable SEI than that of the pristine cathode. Besides, second semicircles of two cathodes in the intermediate frequency (R_{ct}) which is related with charge transfer impedance increase with cycling; however, the R_{ct} values of the silver-coated cathode are much lower than that of the pristine cathode. As seen in Fig. 7 and Table 2, the R_{ct} values of pristine cathode dramatically increased after the first cycle. Electrochemical impedance spectroscopy (EIS) analyses also reveal the more stable electrode/electrolyte interface of the surface-modified electrode for 50 cycles compared with the pristine electrode (Fig. 7) and the semicircle of the silver-coated LMNCO electrode in the EIS curve stays smaller and more steady throughout cycling. The EIS test result verified better electronic conductivity and electrochemical kinetics of the silver-coated cathode [31]. Detailed EIS results are summarized in Table 2.

The values of R_{sf}, R_{ct}, and Li diffusion coefficient (D_{Li}) are shown in Table 2. The diffusion coefficient was extracted according to a Warburg model with a linear overvoltage-current relationship [32–35] using the following equation:

$$D = \frac{R^2 T^2}{2A^2 n^4 F^4 C_{Li}^2 \sigma^2}$$

where R and T are the universal gas constant and the absolute temperature, respectively, A is the surface area of the electrode, n the number of electrons in the electrochemical reaction (1 for Li), F is the Faraday constant, and C_{Li} is the Li-ion concentration in the material. C_{Li} can be depicted as the quotient of density and molar mass and is the Warburg factor which has a relationship with Z_{RE} ($w = 2\pi f$)

$$Z_{RE} = R_{sf} + R_{ct} + \sigma w^{-1/2}$$

The relationship between Z_{RE} and the square root of frequency ($w^{-1/2}$) in the low-frequency region is shown in Fig. 7 d, e as follows:

Figure 7 d, e and Table 2 clearly show that the D_{Li} values of silver-coated cathode material are roughly equal to those of pristine cathode for the first and 10th cycle. The diffusion coefficient of Li ions (D_{Li}) is an intrinsic physical property. As described above, the XRD and SEM analyses showed that silver coating did not change the crystal and particle structures. Because of these reasons, silver coating might not cause a huge change in the D_{Li} values. However, after the 50th cycle, D_{Li} value of silver-coated cathode ($(2.1 \pm 0.2) \times 10^{-15}$ cm^2 s^{-1})) is one order of magnitude higher than that of the pristine cathode ($(8.0 \pm 0.2) \times 10^{-16}$ cm^2 s^{-1}). This issue may be related with two reasons: (i) Li atoms occupy different oxide sites during charge and discharge for the same voltage and/or capacity and (ii) the difficulty for Li^+ trapping in negative SEI film that caused by the crystal structural changes during cycling [36].

Figure 8 shows the capacity cyclability of pristine LMNCO and silver-coated LMNCO at 0.05 C/1 C charge–discharge rate between 2.0 and 4.9 V at 55 °C. It is clear that the silver coating significantly improves the initial discharge capacity of the cathode. However, the surface modification does not

Table 2 Quantitative values of EIS analyses as shown in Fig. 7 b, c

	Pristine LMNCO			Silver-coated LMNCO		
	R_{sf} (Ω)	R_{ct} (Ω)	D_{Li} (cm^2 s^{-1})	R_{sf} (Ω)	R_{ct} (Ω)	D_{Li} (cm^2 s^{-1})
1st cycle	115 ± 3	197 ± 4	$(3.3 \pm 0.1) \times 10^{-15}$	30.4 ± 1.4	66 ± 2	$(7.0 \pm 0.1) \times 10^{-15}$
10th cycle	144 ± 3	311 ± 5	$(1.9 \pm 0.2) \times 10^{-15}$	33.2 ± 1.1	106 ± 3	$(4.6 \pm 0.2) \times 10^{-15}$
50th cycle	180 ± 3	642 ± 4	$(8.0 \pm 0.2) \times 10^{-16}$	33.0 ± 1.3	249 ± 2	$(2.1 \pm 0.2) \times 10^{-15}$

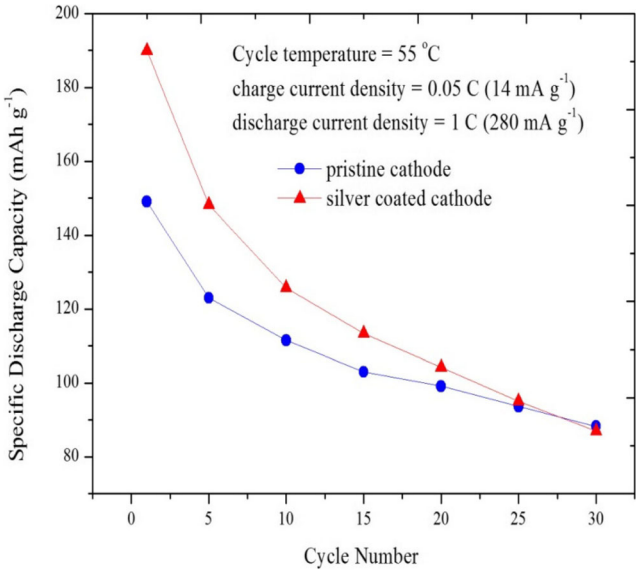

Fig. 8 Discharge capacity as a function of cycle number for the LMNCO and silver-coated LMNCO cathodes at 55 °C in the potential range of 2.0–4.9 V

perform a favorable effect on the cyclability of cathode material at an elevated temperature of 55 °C by contrast with RT. This huge capacity fade of the silver-coated cathode may be related with the decomposition of electrolyte and dissolution of cathode active species in the electrolyte. The released oxygen in the first charge due to the Li_2MnO_3 activation may lead to the formation of H_2O, which can then react with the electrolyte and produce HF [37]. Because HF would etch the electrode surface and deteriorate the electrochemical performance, the primary concern of surface coating is to passivate the electrode surface to avoid the direct contact with HF. Some inorganic materials such as Al_2O_3, ZnO, $AlPO_4$, and AlF_3 that are inert to HF have been investigated as the surface coating layer of LMNCO [38–41]. Unlike the metal oxide coating processes, the silver coating does not act as protective layers on the cathode for the electrolyte. This result shows that the silver coating process enhances the electronic conductivity of cathode material. The high surface electronic conductivity caused by the metal coating reduces cell polarization. The results indicate that such surface treatment of cathode powders should be an effective way to improve cycle-life with higher current retention.

Conclusions

In summary, LMNCO material has been synthesized via a glycine-nitrate combustion method based on the reaction between Mn, Ni, Co acetate, and nitrates and Li_2CO_3. Then, the LMNCO cathode active material coated with silver, as an electronic conductor, notably improves the electronic conductivity on the surface of the electrode. Both the cycling and rate capabilities of the LMNCO cathode material were greatly improved by the silver coating. In addition, the silver coating also reduced the polarization of the electrode and retarded voltage drop during cycling. Thus, silver, as a novel coating material for lithium-rich cathode material, might also be applicable for ameliorating the electrochemical properties of other cathode or even anode materials for higher performance Li-ion batteries.

References

1. Armand M, Tarascon JM (2008) Building better batteries. Nature 451(7179):652–657
2. Tarascon JM, Armand M (2001) Issues and challenges facing rechargeable lithium batteries. Nature 414(6861):359–367
3. Goodenough JB, Kim Y (2010) Challenges for rechargeable Li batteries. Chem Mater 22(3):587–603
4. Armstrong AR, Bruce PG (1996) Synthesis of layered $LiMnO_2$ as an electrode for rechargeable lithium batteries. Nature 381(6582): 499–500
5. Toprakci O, Toprakci HA, Ying L, Liwen J, Leigang X, Lee H, Zhang S, Zhang X (2013) Synthesis and characterization of $xLi_2MnO_3{\cdot}(1-x)LiMn_{1/3}Ni_{1/3}Co_{1/3}O_2$ composite cathode materials for rechargeable lithium-ion batteries. J Power Sources 241:522–528
6. Yabuuchi N, Ohzuku T (2005) Electrochemical behaviors of $LiCo_{1/3}Ni_{1/3}Mn_{1/3}O_2$ in lithium batteries at elevated temperatures. J Power Sources 146(1-2):636–639
7. Rao CV, Reddy ALM, Ishikawa Y, Ajayan PM (2011) $LiNi_{1/3}Co_{1/3}Mn_{1/3}O_2$–graphene composite as a promising cathode for lithium-ion batteries. ACS Appl Mater Interfaces 3:2966–2972
8. Kim Y (2012) Lithium nickel cobalt manganese oxide synthesized using alkali chloride flux: morphology and performance as a cathode material for lithium ion batteries. ACS Appl Mater Interfaces 4(5):2329–2333
9. Zheng J, Gu M, Xiao J, Zuo P, Wang C, Zhang LG (2013) Corrosion/fragmentation of layered composite cathode and related capacity/voltage fading during cycling process. Nano Lett 13(8): 3824–3830
10. Ates MN, Mukerjee S, Abraham KM (2015) A search for the optimum lithium rich layered metal oxide cathode material for Li-ion batteries. J Electrochem Soc 162(7):A1236–A1245
11. Martha SK, Nanda J, Veith GM, Dudney NJ (2012) Electrochemical and rate performance study of high-voltage lithium-rich composition: $Li_{1.2}Mn_{0.525}Ni_{0.175}Co_{0.1}O_2$. J Power Sources 199:220–226
12. Xiao X, Lu P, Ahn D (2011) Ultra thin multifunctional oxide coatings for lithium ion batteries. Adv Mater 23(34):3911–3915
13. Aurbach D (2003) Electrode–solution interactions in Li-ion batteries: a short summary and new insights. J Power Sources 119:497–503
14. Arai H, Tsuda M, Saito K, Hayashi M, Sakurai Y (2002) Thermal reactions between delithiated lithium nickelate and electrolyte solutions. J Electrochem Soc 149(4):A401–A406
15. Ates MN, Shah A, Mukerjee S, Abraham KM (2014) Mitigation of layered to spinel conversion of a Li-rich layered metal oxide cathode material for Li-ion batteries. J Electrochem Soc 161(3):A290–A301
16. Zhang X, Belharouak I, Li L, Lei Y, Elam JV, Nie A, Chen X, Yassar R (2013) Structural and electrochemical study of Al_2O_3 and TiO_2 coated $Li_{1.2}Ni_{0.13}Mn_{0.54}Co_{0.13}O_2$ cathode material using ALD. Adv Energy Mater 3(10):1299–1307

17. Zhao J, Aziz S, Wang Y (2014) Hierarchical functional layers on high-capacity lithium-excess cathodes for superior lithium ion batteries. J Power Sources 275:95–104
18. Wu F, Wang Z, Su Y, Yan N, Bao L, Chen S (2014) $Li[Li_{0.2}Mn_{0.54}Ni_{0.13}Co_{0.13}]O_2$–$MoO_3$ composite cathodes with low irreversible capacity loss for lithium ion batteries. J Power Sources 247:20–25
19. Sun YK, Lee MJ, Yoon CS, Hassoun J, Amine K, Scrosati B (2012) The role of AlF_3 coatings in improving electrochemical cycling of Li-enriched nickel-manganese oxide electrodes for Li-ion batteries. Adv Mater 24(9):1192–1196
20. Son JT, Park KS, Kim HG, Chung HT (2004) Surface-modification of $LiMn_2O_4$ with a silver-metal coating. J Power Sources 126(1-2): 182–185
21. Göktepe H, Şahan H, Patat S (2016) Effect of silver and carbon double coating on the electrochemical performance of $LiFePO_4$ cathode material for lithium ion batteries. Int J Hydrog Energy 41(23):9774–9779
22. Stern KH (2000) High temperature properties and thermal decomposition of inorganic salts with oxyanions. CRC Press, New York
23. Lu ZH, Beaulieu YL, Donaberger RA, Thomas CL, Dahn JR (2002) Synthesis structure and electrochemical behavior of $Li[Ni_xLi_{1/3-2x/3}Mn_{2/3-x/3}]O_2$. J Electrochem Soc 149(6):A778–A791
24. Liu ZL, Yu AS, Lee JY (1999) Synthesis and characterization of $LiNi_{1-x-y}Co_xMn_yO_2$ as the cathode materials of secondary lithium batteries. J Power Sources 81:416–419
25. Yoon WS, Kim N, Yang XQ, McBreen J, Grey CP (2003) 6Li MAS NMR and in situ X-ray studies of lithium nickel manganese oxides. J Power Sources 119:649–653
26. Shen CH, Wang Q, Fu F, Huang L, Lin Z, Shen SY, Su H, Zheng XM, Xu BB, Li JT, Sun SG (2014) Facile synthesis of the Li-rich layered oxide $Li_{1.23}Ni_{0.09}Co_{0.12}Mn_{0.56}O_2$ with superior lithium storage performance and new insights into structural transformation of the layered oxide material during charge–discharge cycle: in situ XRD characterization. ACS Appl Mater Interfaces 6(8):5516–5524
27. Ates MN, Mukerjee S, Abraham KM (2015) A high rate Li-rich layered MNC cathode material for lithium-ion batteries. RCS Adv 5:27375–27386
28. Thackeray MM, Christopher CS, Johnson S (2005) Advances in manganese-oxide composite electrodes for lithium-ion batteries. J Mater Chem 15(23):2257–2267
29. Lin J, Mu D, Jin Y, Wu B, Ma Y (2013) Li-rich layered composite $Li[Li_{0.2}Ni_{0.2}Mn_{0.6}]O_2$ synthesized by a novel approach as cathode material for lithium ion battery. J Power Sources 230:76–80
30. Thackeray MM, Kang SH, Johnson CS (2007) Li_2MnO_3-stabilized $LiMO_2$(M = Mn, Ni, Co) electrodes for lithium-ion batteries. J Mater Chem 17(30):3112–3125
31. Tan KS, Reddy MV, Subba GV, Chowdari BV, Tan R (2005) Effect of $AlPO_4$-coating on cathodic behaviour of $Li(Ni_{0.8}Co_{0.2})O_2$. J Power Sources 141(1):129–142
32. Meyers JP, Doyle M, Darling RM, Newman J (2000) The impedance response of a porous electrode composed of intercalation particles. J Electrochem Soc 147(8):2930–2940
33. Bard AJ, Faulkner LR (2001) Electrochemical methods: fundamentals and applications, 2nd edn. Wiley, New York
34. Zhang L, Duan YX, Peng G, Liang G, Huang YH, Jiang Y, Ni S, Li M (2013) Reduced graphene oxide modified Li_2FeSiO_4/C composite with enhanced electrochemical performance as cathode material for lithium ion batteries. ACS Appl Mater Interfaces 5:2304–12309
35. Wang X, Hao H, Liu J, Huang T (2011) A novel method for preparation of macroposous lithium nickel manganese oxygen as cathode material for lithium ion batteries. Electrochim Acta 56(11): 4065–4069
36. Yan J, Liu X, Li B (2014) Recent progress in Li-rich layered oxides as cathode materials for Li-ion batteries. RSC Adv 4(108):63268–63284
37. Deng H, Belharouak I, Yoon CS, Sun YK (2010) High temperature performance of surface-treated $Li_{1.1}(Ni_{0.15}Co_{0.1}Mn_{0.55})O_{1.95}$ layered oxide. J Electrochem Soc 157(10):A1035–A1039
38. Wu Y (2006) A high capacity, surface-modified layered $Li[Li_{(1-x)/3}Mn_{(2-x)/3}Ni_{x/3}Co_{x/3}]O_2$ cathodes with low irreversible capacity loss. Electrochem Solid-State Lett 9(5):A221–A224
39. Liu J, Reeja-Jayan B, Manthiram A (2010) Conductive surface modification with aluminum of high capacity layered $Li[Li_{0.2}Mn_{0.54}Ni_{0.13}Co_{0.13}]O_2$ cathodes. J Phys Chem C 14:9528–9533
40. Sun YK, Lee YS, Yoshio M, Amine K (2002) Synthesis and electrochemical properties of ZnO-coated $LiNi_{0.5}Mn_{1.5}O_4$ spinel as 5 V cathode material for lithium secondary batteries. Electrochem Solid-State Lett 5(5):A99–A102
41. Cho J, Kim TJ, Kim J, Noh M (2004) Synthesis, thermal, and electrochemical properties of $AlPO_4$-coated $LiNi_{0.8}Co_{0.1}Mn_{0.1}O_2$ cathode materials for a Li-ion cell. J Electrochem Soc 11:A1899–A1904